J Nanopart Res (2014) 16:2748
DOI 10.1007/s11051-014-2748-9

RESEARCH PAPER

Synthesis and characterization of silver colloidal nanoparticles with different coatings for SERS application

L. Mikac · M. Ivanda · M. Gotić · T. Mihelj · L. Horvat

Received: 13 February 2014 / Accepted: 12 November 2014
© European Union 2014

Abstract Silver colloids were produced by chemical reduction of silver salt (silver nitrate, $AgNO_3$) solution. As reducing agents, trisodium citrate, sodium borohydride, ascorbic acid, polyvinylpyrrolidone, and glucose were used. The colloids were characterized by UV–Vis, DLS, zeta potential measurements, and SEM. The colloids were stabilized with negative groups or large molecules attached to their surface. The surface-enhanced Raman scattering (SERS) effect of stabilized nanoparticles was measured by using pyridine and rhodamine 6G molecules as analytes and $NaNO_3$, KCl, and KBr at different concentrations as aggregating agents. The best Raman signal enhancement was achieved using silver nanoparticles of 40 nm size reduced and stabilized with citrate. The SERS signal of analyte molecules was further enhanced with the addition of sodium borohydride as an alternative aggregating agent. The borohydride had the strongest impact on the SERS effect of the colloid consistent of large (0.5 μm) silver nanoparticles stabilized with aminodextran. The mixture colloid-borohydride-pyridine was stable for hours. The mechanism of borohydride in the colloids is discussed.

Keywords Silver nanoparticles · Colloid · Reducing agents · Aggregating agents · SERS · Pyridine

Electronic supplementary material The online version of this article (doi:10.1007/s11051-014-2748-9) contains supplementary material, which is available to authorized users.

L. Mikac · M. Ivanda (✉)
Laboratory for Molecular Physics, Ruđer Bošković Institute, Bijenička c. 54, Zagreb, Croatia
e-mail: ivanda@irb.hr

M. Gotić
Laboratory for Synthesis of New Materials, Ruđer Bošković Institute, Bijenička c. 54, Zagreb, Croatia

T. Mihelj
Laboratory for Synthesis and Processes of Self-assembling of Organic Molecules, Ruđer Bošković Institute, Bijenička c. 54, Zagreb, Croatia

L. Horvat
Laboratory for Electron Microscopy, Ruđer Bošković Institute, Bijenička c. 54, Zagreb, Croatia

Introduction

During the past decades, metal nanostructures received great interest in many fields due to their interesting optical and electric properties. They have been used in electronics (Li et al. 2005), catalysis (Mallick et al. 2006), biomedicine (Thanh and Green 2010), and surface-enhanced Raman scattering (SERS) (Xu et al. 1999), (Ru and Etchegoin 2009). There is particular interest in silver nanostructures due to their outstanding plasmonic properties which lead to a great enhancement of the Raman signal. SERS is an advanced Raman technique that enhances the vibrational spectrum of molecules adsorbed on or in the vicinity of metal particles.

Published online: 11 December 2014

It is currently accepted that two mechanisms, electromagnetic and chemical, contribute to the SERS enhancement (Aroca 2007). In the electromagnetic mechanism, the laser light excites collective oscillations of the surface electrons in a metal which results in the enhancement of the local electromagnetic field. The molecule which is near the metal surface or adsorbed to it experiences this enhancement, and as a result, the intensity of the Raman scattered light is enhanced. In the chemical mechanism, which is usually regarded as weaker than electromagnetic, the polarizability of the molecule adsorbed on the metal surface increases. The total Raman signal enhancement is the product of both processes. In recent times, a significant enhancement of the Raman signal has also been obtained from surfaces of oxide nanosensors (α-Fe_2O_3 thin films) (Fu et al. 2011), which indicates the importance of the chemical enhancement. Because of its readiness, sensitivity, and minimum sample preparation requirements, SERS is being considered as a powerful technique for detection of wide variety of analytes at very low concentrations, even down to the single molecule level (Kneipp et al. 1997).

The main issue today is the synthesis of metal (Ag, Au, Cu) nanoparticles with tunable size, shape, and morphology (Wiley et al. 2006). Silver colloids are usually synthesized by in situ reduction methods, such as chemical reduction, photo reduction (Jia et al. 2006), electrochemical reduction (Yin et al. 2003), or thermal decomposition (Jung et al. 2009). Chemical reduction involves the reduction of a silver salt with a reducing agent in the presence of stabilizer. The most used methods for the preparation of silver nanoparticles in aqueous solution are reduction of silver nitrate, $AgNO_3$, using reducing agents such as citrate (Munro et al. 1995; Rivas et al. 2001), ascorbic acid (Sondi et al. 2003), or borohydride (Dong et al. 2010). The purity of water and reagents, cleanliness of the glassware, and solution temperature are critical parameters in the synthesis process. In addition, the nanoparticles prepared by chemical reduction are usually mixtures of spherical and rod-like silver particles due to the poor balance of nucleation and growth processes (Dong et al. 2009). Nevertheless, due to simplicity of preparation and the fact that they offer fairly good SERS enhancement (up to 10^6) under acceptably reproducible experimental conditions, silver colloids with stabilizing agents have been widely used. The stabilizing agents are chemicals used in the synthesis of nanoparticles that prevent their aggregation through electrostatic or steric repulsion (or both). In the case of silver colloids, most commonly used stabilizing agents are citrate, sodium borohydride, polyvinylpyrrolidone (PVP), and CTAB. According to the type of stabilizing agent, particles of varying size, shape, and stability are obtained. Furthermore, colloidal stability is a function of many factors like the type of stabilizing agent, pH, and ionic strength.

In this work, silver nanoparticles with controlled particle size were prepared using different reducing and stabilizing agents. The silver colloid reduced with citrate was prepared because citrate colloids are most researched and proven to be effective and stable. Due to the difficulties in controlling the hydrolysis of Ag ions, citrate colloids usually have broad size distribution of the synthesized nanoparticles. To address this problem, sample reduced with ascorbic acid was made which proved to result in the formation of uniform nanoparticles. Moreover, the synthesis takes place at room temperature. The sample reduced with borohydride was prepared to avoid the existence of the citrate ions on the surface of the nanoparticles which can lead to reduced adsorption of the analyte. Furthermore, Ag nanoparticles sterically stabilized with polysaccharide aminodextran were investigated because cross-linked aminodextran coating acts as an excellent protecting agent. Besides, these particles have many potential medical applications. The nanoparticles stabilized with biodegradable polymer PVP as well have an important medical role, for example, as a linker for binding drugs (Patil et al. 2009). The morphological properties of the particles obtained with different chemical synthesis were studied and their influence on SERS was shown.

Experimental section

Materials

Silver nitrate ($AgNO_3$) (Kemika), trisodium citrate ($Na_3C_6H_5O_7$) (Kemika), sodium borohydride ($NaBH_4$) (Kemika), L-(+)-ascorbic acid ($C_6H_8O_6$) (Kemika), DEAE-dextran hydrochloride (aminodextran) (Sigma-Aldrich), β-D(+)glucose (Sigma-Aldrich), PVP (average mol wt 10,000) (Sigma-Aldrich), sodium hydroxide (NaOH) (Kemika), KCl (Kemika), KBr (Fluka), $NaNO_3$ (Kemika), pyridine

(Kemika), and rhodamine 6G (R6G) (Exciton) were of analytical grade and were used without further purification. High-purity water with a resistivity of 18 MΩ cm was used in all experiments.

Preparation of silver nanoparticles using citrate (AGC)

Sample AGC was prepared using chemical reduction method according to the slightly modified method of Lee and Meisel (Lee and Meisel 1982). In this experiment, 90 mg of $AgNO_3$ in 500 mL of miliQ H_2O was poured into four-neck glass flask and heated with permanent stirring with glass stirrer to boiling in an oil bath (120 °C) under reflux and nitrogen bubbling. To this solution, 50 mL of 1 % trisodium citrate was added rapidly. During the process, solution was mixed vigorously. Solution was refluxed at 120 °C for 90 min, and the color was turbid gray. Then the mixture was removed from the oil bath and stirred until cooled to room temperature.

Preparation of silver nanoparticles using ascorbic acid (AGA)

Sample AGA was synthesized using ascorbic acid as reducing agent and citrate as stabilizer (Qin et al. 2010). Typically, a 160 mL aqueous solution containing ascorbic acid (6.0×10^{-4} M) and trisodium citrate (3.0×10^{-3} M) was adjusted to pH 9–10 by addition of 1 M NaOH solution. The 1.6 mL of 0.1 M aqueous solution of $AgNO_3$ was added under a stirring to a flask maintained at 30 °C in an oil bath. After 15 min, the reaction solution color was brown indicating that the reactions were completed.

Preparation of silver nanoparticles using borohydride (AGBH)

Sample AGBH was synthesized using ice-cold sodium borohydride (Creighton et al. 1979; Suh et al. 1983). A large excess of sodium borohydride is needed both to reduce the ionic silver and to stabilize the formed nanoparticles. 30 mL of 0.002 M sodium borohydride ($NaBH_4$) was added to an Erlenmeyer flask which was placed in an ice bath and stirred constantly for about 30 min. 10 mL of 0.001 M silver nitrate ($AgNO_3$) was added dropwise into the stirring $NaBH_4$ solution. Stirring was stopped as soon as all of the $AgNO_3$ is added. The color of the solution changed from colorless to dark yellow.

Preparation of silver nanoparticles stabilized with dextran (AGD)

Sample AGD was synthesized using sodium borohydride as reducing agent in the presence of dextran as stabilizer (Yang et al. 2012). In details, dextran was dissolved in 12 mL of 50 mM $AgNO_3$ aqueous solution ($AgNO_3$/dextran = 1:2 by weight). The solution was stirred until it became homogenous. Then, obtained mixture was added dropwise to 48 mL of freshly prepared 20 mM $NaBH_4$ solution that had been cooled in an ice bath. During the addition of borohydride, the reaction mixture was stirred vigorously on a magnetic stir plate. It was observed that the color of the solution changed from colorless to light yellow and finally to dark green.

Preparation of silver nanoparticles stabilized with PVP (AGP)

Sample AGP was prepared from the solutions of 0.3 M of $AgNO_3$ and 5 wt% PVP in distilled water (Lee et al. 2010). 2.5 g of PVP was dissolved in 50 mL of distilled water, and afterwards, 2.55 g of silver nitrate was added to the solution. The color of the solution changed from light yellow to dark brown. The chemical process lasted 2 h at room temperature.

Preparation of silver nanoparticles using glucose (AGG)

Sample AGG was prepared by reducing the silver nitrate with glucose in PVP aqueous solution with sodium hydroxide which accelerates the reaction (Wang et al. 2005). The PVP solution was prepared by dissolving PVP, glucose, and sodium hydroxide in 15 mL of M-Q water. This solution was stirred and heated to 60 °C. 5 mL of 0.01 M $AgNO_3$ was added into PVP solution drop by drop. After the addition of silver nitrate, the solution was stirred for ten more minutes. The final color of the solution was dark red.

Nanoparticles characterization

The absorption optical spectra of silver samples were recorded using UV–Vis–NIR spectrophotometer (UV-

3600, Shimadzu). All the spectra were recorded at room temperature.

The morphology of silver nanoparticles in silver samples was investigated with Jeol JSM 7000F field emission scanning electron microscope (FE-SEM) coupled with Energy-dispersive spectroscopy (EDS). 10 μL of colloid solution was pipetted on silicon wafer and allowed to dry in ambient conditions. Using ImageJ software, the particle size distribution was determined. TEM micrographs were acquired on a Zeiss EM10 microscope.

Dynamic light scattering (DLS) measurements were performed by a Zetasizer Nano ZS (Malvern Instruments, UK) equipped with a 532 nm "green" laser. Size distributions given by DLS were reported as volume distribution, and results are presented as the mean value of at least six measurements. Zeta potential was taken as the mean value of six measurements.

The pH measurements were made using pH meter calibrated with 4.005 and 7.00 buffer solutions. All measurements were conducted under room temperature.

The Raman spectra were recorded by Horiba Jobin–Yvon T64000 triple Raman spectrometer in the subtractive mode. The 488 and 514.5 nm argon ion laser and 532 diode laser were used. The colloid-aggregating agent-analyte solution (0.1 mL) was vortexed for 30 s and then placed in a glass capillary (25 × 2 mm) and positioned in the macro chamber of the Raman instrument. The laser beam was focused with 100 mm lens in 90° geometry. The laser power on the sample was approximately 60 mW. Raman scattering experiments were carried out at room temperature. Spectra were recorded with the CCD detector immediately after positioning the sample with 30 s accumulations and three replicates unless stated otherwise. The spectral region of investigation was 950–1,100 cm^{-1} where the lines of two ring breathing modes, ν_1 and ν_{12}, are expected (Heaviside et al. 1981). All colloids were stored at 4 °C and prior to their use were allowed to reach room temperature for at least 1 h. The colloids were gently shaken before the experiments to avoid any effects of sedimentation. In order to achieve about the same concentrations of the colloids, the AGD, AGP, and AGG colloids were diluted with ultra pure water (AGDd, AGPd, and AGGd) and colloid AGBH was concentrated by centrifugation (12,000 rpm, 15 min) and redispersion in smaller volume of ultra pure water (AGBHc).

Results and discussion

Colloid characterization

Figure 1 shows UV–Vis spectra of the synthesized silver nanoparticles in the range from 200 to 800 nm. The absorption band in visible light region from 350 to 550 nm is typical for silver nanoparticles, and the samples AGC, AGA, AGBH, and AGD have the absorption maximum at 407, 402, 390, and 410 nm, respectively. AGC sample has the broadest band indicating non-uniform distribution of silver nanoparticles. Samples AGA, AGBH, and AGD have smaller values of absorption peak FWHM indicative of a narrow size distribution. In the case of samples which are stabilized with PVP (AGP and AGG), the maximum of absorption is masked with the absorption of polymer molecules. The absorption band of silver nanoparticles appears as a shoulder and is marked with an arrow in Fig. 1.

FE-SEM and TEM measurements were carried out to observe the size and morphology of the silver nanoparticles prepared with different reducing and stabilizing agents. Figure 2 shows SEM images of synthesized nanoparticles. The sample AGC prepared with citrate (Fig. 2a) consists of quasi-regular spherical nanoparticles with small amount of rod-like nanoparticles. The presence of rod-like nanoparticles as an impurity is difficult to avoid due to poor control of Ag NPs morphology when only citrate is used in the synthesis. Figure 2b shows rather uniform NPs, 17 nm in size, that were obtained by the ascorbic acid/citrate

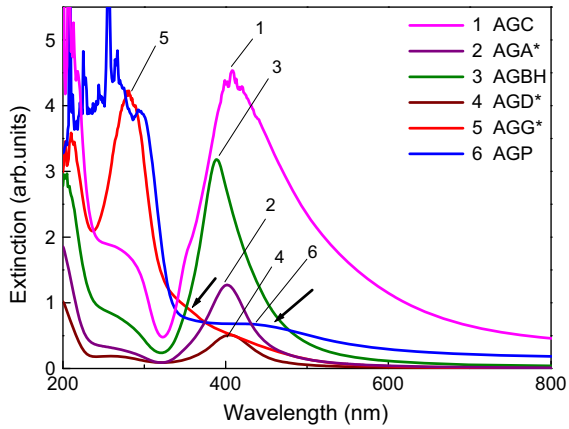

Fig. 1 UV–Vis spectra of the silver nanoparticles synthesized. The samples marked with *asterisk* were diluted with water (sample AGA ten times; samples AGD and AGG 300 times)

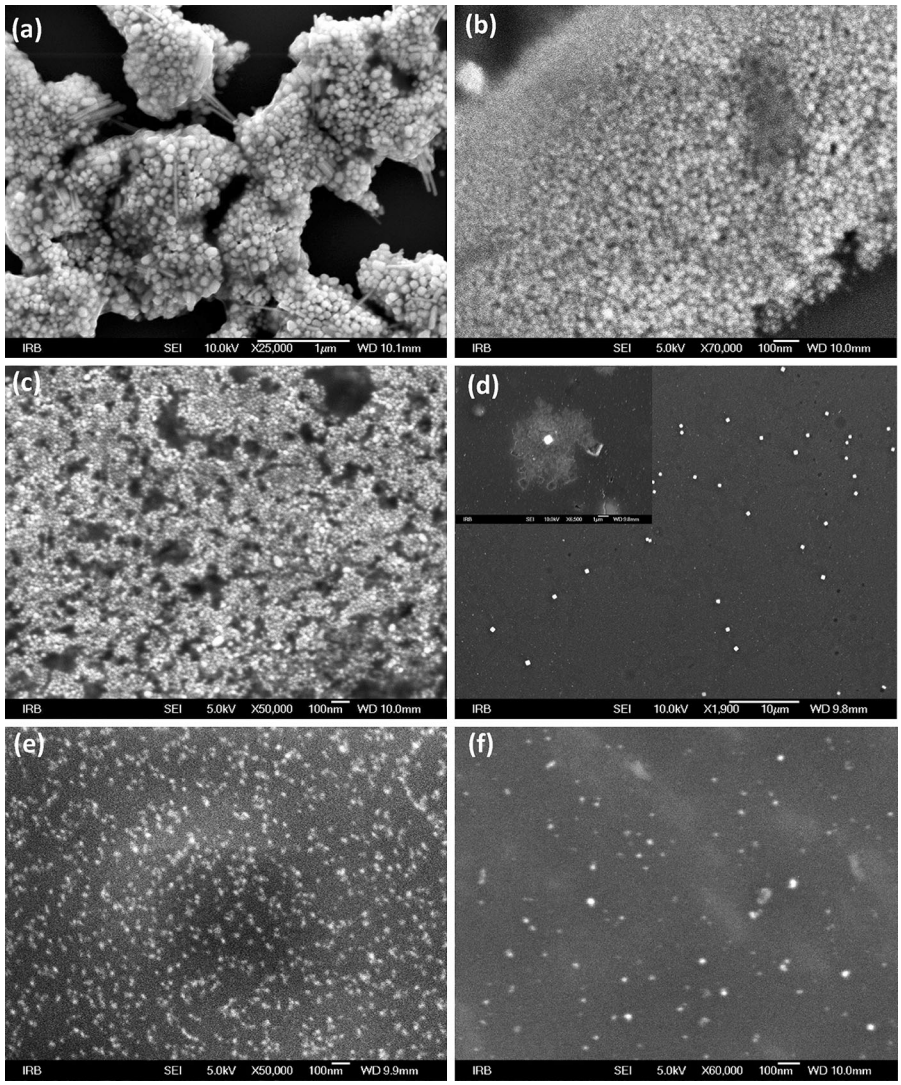

Fig. 2 SEM images of **a** AGC, **b** AGA, **c** AGBH, **d** AGD, **e** AGP, and **f** AGG sample

synthesis (sample AGA). Figure 2 c shows 11 nm NPs obtained by reduction with $NaBH_4$ (sample AGBH). Figure 2d shows SEM image of sample AGD that was obtained in the presence of robust high-molecular-weight aminodextran polymer. The large NPs of about 500 nm and much smaller light dots that may correspond to tiny silver NPs are visible. Figure 2e shows the 12 nm NPs obtained in the presence of PVP, whereas the 13 nm NPs synthesized in the glucose/PVP mixture are shown in Fig. 2f.

TEM micrographs were taken for AGA, AGBH, AGG, and AGP samples (Fig. 3) where SEM images were not of satisfying quality and it was difficult to measure the particles diameters. TEM images reveal nice spherical particles obtained in AGA and AGBH samples. AGG sample has a complicated organic matrix and had to be diluted in order to see and measure the diameter of silver nanoparticles. In AGP sample, some triangular-shaped particles can also be noticed.

The particle size distributions calculated from the corresponding SEM and TEM images using ImageJ computer program are shown in Online resource. The calculated mean particle sizes and their standard deviation are given in Table 1. The particle size distributions obtained from SEM and TEM images are

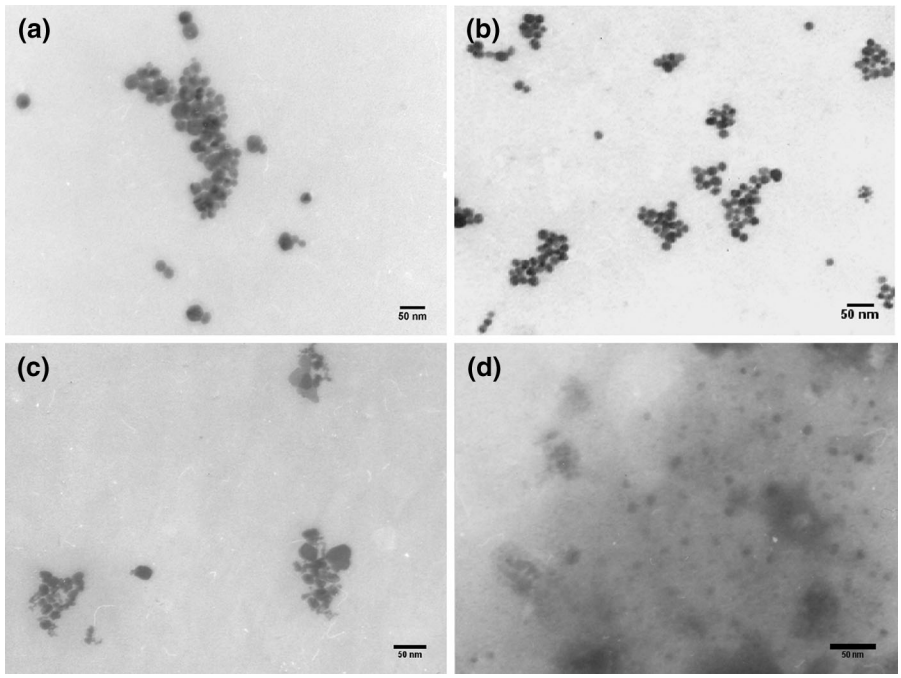

Fig. 3 TEM images of **a** AGA, **b** AGBH, **c** AGP, and **d** AGG samples

not very different, and the biggest difference in particle size was calculated for AGG sample. Also, the hydrodynamic diameters and zeta potential results of DLS measurements are given in Table 1. Typically, nanoparticles with zeta potentials greater than 20 mV or less than −20 mV (or ±30 mV depending on the literature source) have sufficient electrostatic repulsion to remain stable in solution. The samples AGC, AGA, and AGD are above or below this value and can all be considered as stable without tendency to aggregate spontaneously. The silver nanoparticles in AGC and AGA samples are stabilized with adsorbed negative citrate ions that cause repulsive force along particles and prevent aggregation while AGD sample is stabilized sterically and with positive diethylaminoethyl-dextran molecules. The negative zeta

Table 1 Characterization of the prepared silver samples

Sample	Reducing/ stabilizing agent	SEM (nm) TEM (nm)	Zeta (mV)	Hydrodynamic diameter (nm)	UV–Vis–NIR (nm)	FWHM	Total Ag concentration (mg L^{-1})	pH
AGC	Citrate/citrate	35.8 ± 6.3	−33.4	14.6; 69.8	407	139	104	7.7
AGA	Ascorbic acid/citrate	16.7 ± 4.4 13.1 ± 4.3	−46.8	5.4	402	62	107	7.9
AGBH	$NaBH_4/BH^{4-}$	10.9 ± 2.9 12.1 ± 3.3	−10.1	2.87	390	62	27	7.5
AGD	$NaBH_4$/DEAE-dextran	518 ± 114	39.5	473	410	60	10^3	8.2
AGP	PVP/PVP	11.6 ± 4.1 10.3 ± 4.0	−0.867	4.62	420	–	3×10^4	5.6
AGG	Glucose/PVP	12.6 ± 4.2 5.8 ± 1.9	−11.2	14.28	283	–	270	7.9

At least fifty nanoparticles were measured by SEM or TEM to calculate the mean and SD of the size

potential of sample AGBH indicates the NPs stabilization with negative BH^{4-} groups. The PVP-stabilized samples (AGP and AGG) have a slightly negative zeta value that implies formation of negative charge on the nanoparticle surface. Thus, besides the suppression of agglomeration by steric shielding, the colloidal stability is increased by electrostatic repulsion.

The hydrodynamic diameter values in most cases are slightly lower than the diameter calculated from SEM images. Because the exact shape and hydrodynamic properties of nanoparticulate aggregates are not well known, there may be systematic differences between the calculated RH and spatial dimensions observed by SEM microscopy. Air-dried colloids for SEM measurements are probably not a good representative of the same colloids in aqueous suspension. In the case of AGC sample, there are two diameter values which indicate that in addition to the silver spheres, rod-like particles are also synthesized.

SERS measurements

The performances of the colloids were evaluated by their SERS activity using pyridine. To determine the suitable volume of colloid for further analysis, different volumes of AGC, AGA, AGDd, and AGBHc samples were tested using 10 μL of 0.12 M pyridine (AGC and AGA) and 10 μL of 1.2 M pyridine (AGDd and AGBHc). Figure 4 shows the results. We can see that there is an increase in intensity with increase of the volume for AGC sample up to the volume of 7 μL and after 100 μL the intensity of the band significantly declines. Between these volumes, points deviate so we cannot tell where the real maximum of intensity is. The situation is clear for the other two samples, AGA and AGDd, where the maximum of intensity can be clearly seen (30 μL). For AGBHc sample, it is not easy to tell where the maximum is since the intensity values are not changed significantly with the change in volume of the colloid for the tested range.

The SERS spectra of pyridine were also detected using KBr, KCl, and $NaNO_3$ in 0.01, 0.1, and 1 M concentrations and $NaBH_4$ in 0.1 M concentration to find the optimal aggregating agent as well as optimum concentration for SERS enhancement. Four types of samples were tested: AGC, AGA (0.12 M pyridine used), AGBHc, and AGDd (1.2 M pyridine used). Figure 5 shows the intensity of SERS signal of

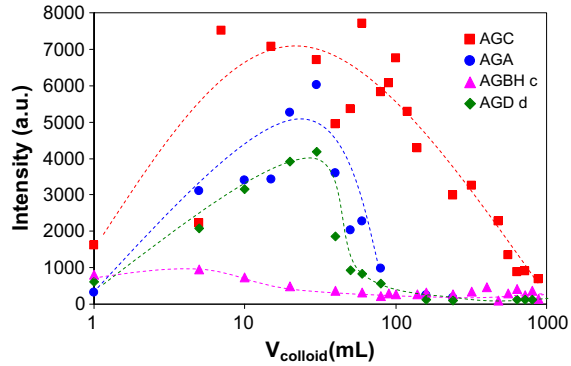

Fig. 4 Pyridine SERS intensities of the band at 1,008 cm^{-1} as a function of colloid volume in the log scale from 1 to 900 μL. The *dashed lines* are added as a visual help. (*Note* the ratio of aggregating agent and colloid was maintained constant throughout the experiment)

pyridine when different aggregating agents were used. The intensity was enhanced significantly when Br^-, Cl^-, or NO_3^- ions were added to the sample which confirms that the aggregation or change in the surface chemistry of nanoparticles occured. In terms of concentration, in the case of KBr, KCl, and $NaNO_3$, 1 M concentrations give much greater enhancement for AGC and AGA samples, while 0.1 M concentrations give the highest enhancement for AGBHc and AGDd samples. Among the three kinds of anions, NO_3^- (1 M) gives the greatest enhancement on SERS signal for ascorbic acid-reduced samples, and Br^- (1 M) for

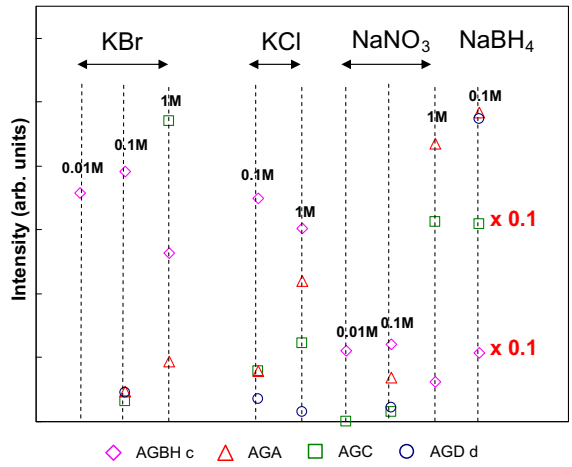

Fig. 5 Pyridine SERS intensities at 1,008 cm^{-1} as a function of different aggregating agents and their concentrations for AGC, AGA, AGBHc, and AGDd samples. (*Note* the concentration of pyridine was maintained constant throughout the experiment.)

citrate-reduced sample. The addition on borohydride resulted in very good enhancement of Raman signal for AGA, AGDd, and AGBHc samples and huge enhancement for AGC sample. The differences of the SERS spectra of pyridine when adding different types and concentrations of ions to the colloids may be attributed to the both effects of degree of aggregation of the colloid and the change on the surface of silver structures (Schluecker and Kiefer 2010). However, the phenomenon of different enhancement when various anions are added to colloids is not yet completely understood (Yaffe and Blanch 2008).

To evaluate the concentration dependence of the Raman signal intensity of the analyte, SERS spectra of two selected analytes, pyridine and rhodamine 6G, were collected. Figure 6a shows enhanced Raman intensities as a function of concentration for two pyridine bands at two excitation wavelengths. Both of our analytes form a complex with silver nanoparticles in the colloids, that is, their adsorption to the NPs surface is enabled by creation of van der Waals interactions. The adsorption is characterized by one of the adsorption isotherms which describe the surface coverage as a function of the pressure or concentration (Langmuir adsorption isotherm being the simplest). In the SERS measurements, when intensity reaches the maximum value at the saturated concentration of the analyte, i.e., when the adsorbate forms a monolayer on NPs surface, the surface coverage also obtains its maximum value. Thus, the concentration-dependent calibration curve can be explained by a Langmuir adsorption isotherm (Schmidt et al. 2004):

$$I = \frac{I_{\max} Kc}{1 + Kc}, \tag{1}$$

where I, $I_{\max}$, K, and c are Raman intensity of the analyte, maximum value of the SERS intensity, analyte concentration, and adsorption constant, respectively. At low concentration range with K^*c much smaller than 1, Eq. (1) is of linear form and its slope is $K^*I_{\max}$.

Applying the formula (1) to fit the experimental points, the adsorption constants, K, and SERS maximum values, $I_{\max}$, of pyridine and R6G were obtained. Figure 6b shows an example of concentration-dependent calibration curve drawn based on the method mentioned above. The adsorption constants and SERS maximum values were calculated for two pyridine bands (1,008 and 1,036 cm^{-1}) and two R6G bands (612 and 776 cm^{-1}) at three excitation wavelengths (488, 532, and 514.5 nm) with the addition of nitrate and borohydride to AGC, AGA, AGBHc, and AGDd samples. The results are summarized in Table 2.

From the results in Table 2, we can see that colloid-pyridine samples where borohydride is added achieve higher $I_{\max}$ values than those samples where nitrate (or without aggregating agent) is added (all SERS spectra are given in SI, Figs. 1–12). High $I_{\max}$ values for R6G are partially due to resonant Raman effect for these excitation wavelengths.

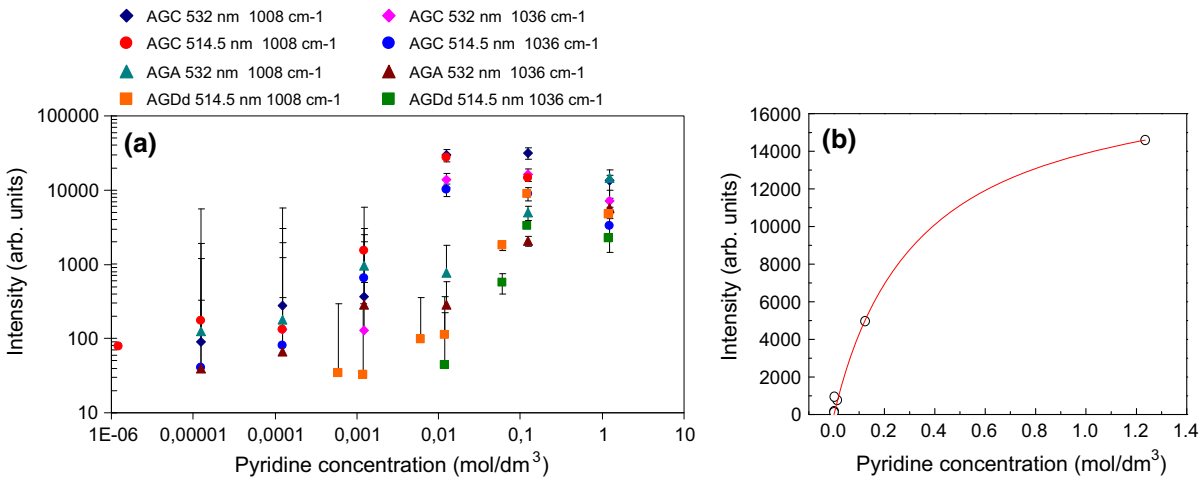

Fig. 6 **a** Pyridine SERS intensities (with *error bars*) at 1,008 and 1,036 cm^{-1} as a function of pyridine concentration in log–log scale in AGC, AGA, and AGDd. **b** Calibration of SERS intensity of pyridine (1,008 cm^{-1}) in AGA sample at 532 nm versus its concentration according to the Langmuir isotherm

The SERS enhancement factor values were calculated by comparing the intensity of the appropriate pyridine peak ($\sim$1,008 cm^{-1}) measured in the SERS experiments to the corresponding peak measured from an aqueous solution of pyridine.

The SERS enhancement factor is defined as

$$EF = \frac{I_{SERS}}{I_{NR}} \times \frac{c_{NR}}{c_{SERS}}, \quad (2)$$

where I_{SERS} and I_{NR} are intensities of the band of pyridine in the SERS spectrum and in the normal Raman spectrum, respectively (in this case 1,008 cm^{-1}) and c is the pyridine concentration in the aqueous solution (c_{NR}) or in the colloid (c_{SERS}). This equation can be expanded to take into account the number of molecules in laser activation volume:

$$EF = \frac{I_{SERS}}{I_{NR}} \times \frac{c_{NR}}{c_{SERS}} \times \frac{N\text{py}}{N_{NP-py}}, \quad (3)$$

N_{py} and $N_{NP\text{-}py}$ are number of pyridine molecules in aqueous solution and number of pyridine molecules adsorbed on the silver nanoparticles, respectively, in the laser activation volume. The laser activation volume was estimated to be 9.8×10^{-7} cm^3 considering 500 μm optical path in a 50-μm-sized laser spot. The number of pyridine molecules (N_{py}) existing in laser activation volume at 0.1235 M is 7.35×10^{13}. Knowing the volume of an Ag atom ($V_{Ag} = 1.713 \times 10^{-2}$ nm^3) and calculating the volume of silver nanoparticle for AGC sample (considering a diameter of 36 nm), we can calculate the number of Ag atoms per nanoparticle (1.42×10^6). The number of silver atoms in the laser activation volume is 5.68×10^{11} at

Table 2 The R^2 values, adsorption constants, and maximum SERS intensities calculated for two pyridine bands (1,008 and 1,036 cm^{-1}) and two R6G bands (612 and 776 cm^{-1}) at three excitation wavelengths (488, 532, and 514.5 nm)

λ (nm)	Sample		ν (cm^{-1})	R^2	I_{max}	K
532	AGC	Pyridine (+nitrate)	1,008	0.99604	7260 ± 570	23 ± 5
			1,036	0.99351	3,220 ± 190	91 ± 21
		Pyridine (+borohydride)	1,008	0.93671	35,400 ± 5,500	185 ± 130
			1,036	0.94419	17,800 ± 2,900	159 ± 115
		R6G (+borohydride)	612	0.99993	621,000 ± 29,000	6,748 ± 523
			776	0.99995	727,000 ± 80,000	3,016 ± 430
	AGA	Pyridine	1,008	0.99780	5,880 (K^*I_{max})	
			1,036	0.98690	5,740 (K^*I_{max})	
		Pyridine (+borohydride)	1,008	0.99486	18,500 ± 1,060	3 ± 0.6
			1,036	0.99712	7,030 ± 290	3.4 ± 0.4
514.5	AGC	Pyridine (+borohydride)	1,008	0.99810	2×10^6(K^*I_{max})	
			1,036	0.90695	10,500 ± 1,880	258 ± 222
		R6G (+borohydride)	612	0.99290	110 (K^*I_{max})	
			776	0.99440	7×10^8 (K^*I_{max})	
	AGBHc	Pyridine (+borohydride)	1,008	0.93786	3,200 ± 220	413 ± 154
			1,036	0.94757	1,430 ± 80	350 ± 110
		R6G (+borohydride)	612	0.99972	44,530 ± 2,320	1.5 x 10^6
			776	0.99988	39,860 ± 1,480	1.4 x 10^6
	AGDd	Pyridine (+borohydride)	1,008	0.99208	5,310 ± 260	7.4 ± 1.4
			1,036	0.99697	2,730 ± 180	4.2 ± 1.1
		Pyridine (+nitrate)	1,008	0.97877	7,530 ± 1,510	1.3 ± 0.6
			1,036	0.97896	2.5×10^4 (K^*I_{max})	
488	AGC	Pyridine (+borohydride)	1,008	0.95949	1,226 ± 150	6.7 ± 3.1
			1,036	0.99276	988 ± 170	1.5 ± 0.6
	AGA	Pyridine(+borohydride)	1,008	0.90809	740 ± 60	610 ± 265
			1,036	0.90132	485 ± 40	360 ± 165

AGC concentration used, so the number of nanoparticles is calculated to be 4×10^5. The total surface available on these nanoparticles is 1.6×10^9 nm^2. Assuming the molecular area of pyridine molecule to be 0.28 nm^2 (calculated from the unit cell parameters) and a full coverage of silver nanoparticles, the number of pyridine molecules adsorbed on the nanoparticles in laser activation volume is 5.8×10^9 ($N_{\text{NP-py}}$). Thus, from the above calculation, we can obtain $N_{\text{py}}/N_{\text{NP-py}}$ ratio of 1.27×10^4.

The best Raman enhancement for pyridine when nitrate was used as aggregating agent (1 M) was noticed for AGC sample and was 2.2×10^2. Taking into account the value of 1.27×10^4 we calculated for $N_{\text{py}}/N_{\text{NP-py}}$ ratio, we obtain EF values which are of the order of 10^6. The samples AGA, AGBH, AGBHc, and AGD showed rather lower enhancement of the signal than AGC. It should be pointed out that the best enhancement for AGA and AGBH samples was achieved without the addition of nitrate possibly due to aggregation induced by pyridine itself. In the samples where nitrate was not added, the band at 1,008 cm^{-1} (ring breathing vibration) was weaker than the band at 1,036 cm^{-1} (ring trigonal deformation). With the addition of nitrate (or other aggregating agents), the relative intensities were reversed which could be an indication of change of the surface charge (Cardini et al. 2007). The samples stabilized with PVP showed no surface enhancement of Raman signal for pyridine, even when the samples were diluted. It is most likely that the native surface species on the prepared samples have a higher binding affinity for silver nanoparticles than pyridine. The limit of detection for pyridine when AGC and AGA samples were used was 1.2×10^{-4} mol/dm^3 while for the aqueous solution, the limit of detection was 0.12 mol/dm^3. AGBH had the limit of detection one order of magnitude higher than AGC and AGA (1.2×10^{-3} mol/dm^3) while AGD had the LOD for pyridine 6×10^{-4} mol/dm^3. For AGD sample, the LOD remained the same even after dilution (AGDd).

When borohydride was added instead of nitrate, the lowest concentration measured was 2 orders of magnitude lower for AGC (1.2×10^{-6} mol/dm^3) and one order of magnitude lower for AGA (1.2×10^{-5} mol/dm^3) than the lowest concentrations measured without borohydride. For the concentrated AGBH sample (AGBHc), the limit of detection was 6×10^{-5} mol/dm^3, and for diluted AGD (AGDd), the LOD was 6×10^{-4} mol/dm^3. As for enhancement factors, the largest change occurred in AGD sample (although in this sample, there was no change in LOD) in which the estimated enhancement factor increased 20 times. AGD seems to be very complex sample that comprises of small silver particles and the large aminodextran-coated particles, and it needs to be explored further. For the other two samples, change in enhancement is slightly weaker, and for AGC, the final enhancement factor was approximately 1.3×10^3.

Addition of $NaBH_4$

Since it was noticed that the addition of sodium borohydride leads to a very good amplification of the Raman signal, we tried to clarify the mechanism of borohydride added to the colloid sample-analyte mixture. Figure 7 shows absorption spectrum of the citrate-reduced silver sample with sodium nitrate and sodium borohydride. It is observed that the addition of 1 M $NaNO_3$ leads to a decrease of absorption in the plasmon resonance region, and new broad band appears in the longer wavelength region. Upon addition of 0.1 M $NaBH_4$, it seems that the position of the absorption band does not change but probably the change in chemical property of the silver surface occurs.

In order to explain the behavior and aggregation of the particles in the colloid, DLS measurements were made during 20 min. Figure 8 shows hydrodynamic diameter of the aggregates formed in AGC and AGA samples when nitrate and borohydride were used as aggregating agents. The addition of borohydride to AGC sample resulted in the formation of a larger

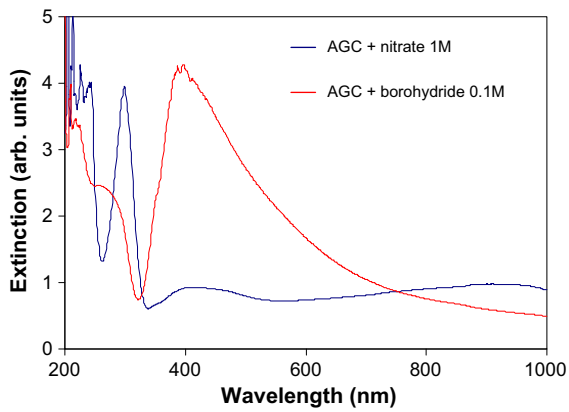

Fig. 7 UV–Vis absorption spectrum of the citrate-reduced silver sample with sodium nitrate (*blue line*) and with sodium borohydride (*red line*). (Color figure online)

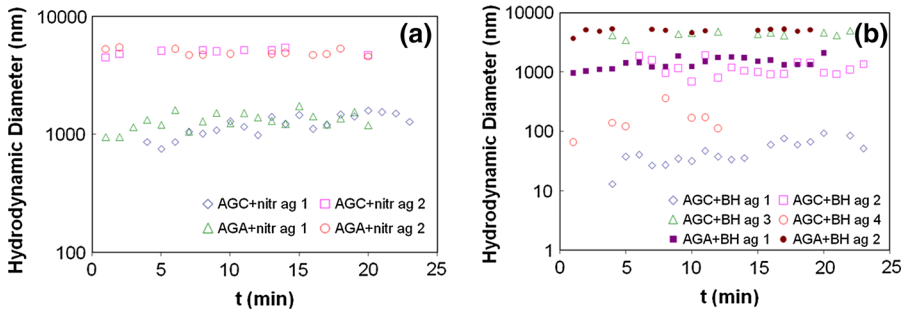

Fig. 8 Aggregation profiles for AGA and AGC samples during time when nitrate (1 M) (**a**) and borohydride (0.1 M) (**b**) were added as aggregating agents

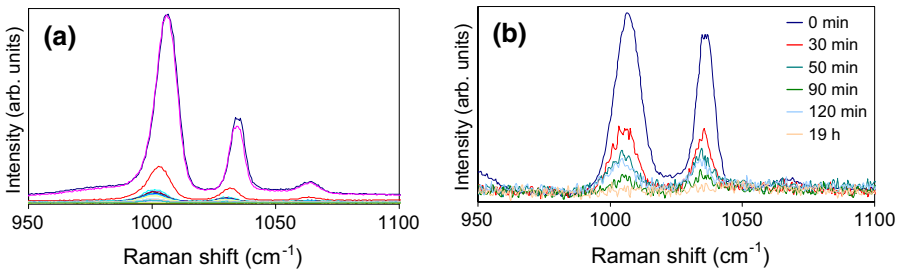

Fig. 9 **a** SERS spectra of pyridine in AGC sample recorded one after another during 25 min after addition of 0.1 M $NaBH_4$ (the highest peak represents the longest time) and **b** SERS spectra of pyridine recorded in 19 h after addition of 1 M $NaNO_3$ (from *top* to *bottom* 0, 30, 50, 90, and 120 min and 19 h, respectively)

number of aggregates of different sizes and some smaller aggregates, compared to AGA sample (Fig. 8b). In the case of nitrate addition, in both samples, two sizes of aggregates were formed. Aggregates tend to grow slowly over time measured. This indicates that a greater enhancement of SERS signal when using AGC sample and $NaBH_4$ may be caused by increasing the number of active sites due to formation of various agglomerates. In addition, the mixture of AGC sample, nitrate, and pyridine has zeta potential very similar to the potential of the AGC sample itself (−34.4 mV). In contrast, the mixture of AGC sample, sodium borohydride, and pyridine has a more negative zeta potential (−42 mV). The addition of different aggregating agents in a greater or lesser extent affects the surface charge of the NP and thus influences the degree of aggregation.

It was also noticed that in contrast to addition of aggregating agents (Cl^-, Br^-, NO_3^-), in the case of $NaBH_4$, the intensity of both observed bands is growing at a time, up to 30 min after the addition of borohydride. Figure 9 shows SERS spectra of pyridine (0.12 M) in AGC sample recorded one after another during 25 min after addition of 0.1 M $NaBH_4$ (a) and SERS spectra of pyridine (0.12 M) recorded in 19 h after addition of 1 M nitrate as aggregating agent (b). This may be explained by the high reactivity of freshly prepared borohydride which probably further reduces the residual silver in the mixture for a certain period of time. Also, if the analysis is repeated in 24 h, there is no significant decrease of the SERS intensity unlike when halide anions or nitrate as aggregating agents are used where the intensity drops to less than half of the initial intensity after 30 min.

Conclusions

A range of silver colloids, prepared by reducing silver nitrate with citrate, ascorbic acid, $NaBH_4$, PVP, and glucose in the presence of stabilizing agents, were investigated with respect to nanoparticle morphology and SERS activity. The results from UV–Vis, zeta potential, DLS, and SEM confirm that stable silver nanoparticles of a certain size and charge are formed. Applying the Langmuir adsorption isotherm, the adsorption constants, K, and SERS maximum values, I_{max}, of pyridine and R6G were obtained. The best Raman enhancement for pyridine was achieved using silver nanoparticles of 40 nm size reduced and stabilized with citrate. The SERS signal of analyte molecules was further enhanced with the addition of

sodium borohydride as an alternative aggregating agent. The lowest limits of detection were obtained with AGC and AGA samples. The SERS enhancement factors for pyridine were calculated taking into account the number of molecules on the silver nanoparticles in laser activation volume and for the best results was estimated to be of the order 10^6.

Acknowledgments This work was supported by the Ministry of Science and Technology of the Republic of Croatia, Project Number 098-0982904- 2898. Financial support by the Croatian Center of Excellence for Advanced Materials and Sensors is gratefully acknowledged. This work was performed in the context of the European COST Action MP1302 Nanospectroscopy.

References

Aroca R (2007) Surface-enhanced raman scattering. In: Surface-enhanced vibrational spectroscopy. Wiley, New York, pp 73–106

Cardini G, Muniz-Miranda M, Pagliai M, Schettino V (2007) A density functional study of the SERS spectra of pyridine adsorbed on silver clusters. Theor Chem Acc 117(3):451–458

Creighton JA, Blatchford CG, Albrecht MG (1979) Plasma resonance enhancement of Raman scattering by pyridine adsorbed on silver or gold sol particles of size comparable to the excitation wavelength. J Chem Soc Farad T 2 75 (0):790–798

Dong X, Ji X, Wu H, Zhao L, Li J, Yang W (2009) Shape control of silver nanoparticles by stepwise citrate reduction. J Phys Chem C 113(16):6573–6576

Dong X, Ji X, Jing J, Li M, Li J, Yang W (2010) Synthesis of triangular silver nanoprisms by stepwise reduction of sodium borohydride and trisodium citrate. J Phys Chem C 114(5):2070–2074

Fu X, Wang S, Zhao Q, Jiang T, Yin H (2011) Thin films of α-Fe2O3 nanoparticles using as nonmetallic SERS-active nanosensors for submicromolar detection. Front Chem China 6(3):206–212

Heaviside J, Hendra PJ, Paul SO, Freeman JJ, Friedman RM (1981) Adsorbate-substrate interaction: a Raman study of pyridine adsorbed on γ-Al2O3 at very low coverages. Appl Spectrosc 35(2):220–222

Jia H, Zeng J, Song W, An J, Zhao B (2006) Preparation of silver nanoparticles by photo-reduction for surface-enhanced Raman scattering. Thin Solid Films 496(2):281–287

Jung YK, Kim JI, Lee J-K (2009) Thermal decomposition mechanism of single-molecule precursors forming metal sulfide nanoparticles. J Am Chem Soc 132(1):178–184

Kneipp K, Wang Y, Kneipp H, Perelman LT, Itzkan I, Dasari RR, Feld MS (1997) Single molecule detection using surface-enhanced Raman scattering (SERS). Phys Rev Lett 78(9):1667–1670

Lee PC, Meisel D (1982) Adsorption and surface-enhanced Raman of dyes on silver and gold sols. J Phys Chem 86(17):3391–3395

Lee CJ, Karim MR, Vasudevan T, Kim HJ, Raushan K, Jung MJ, Kim DY, Lee MS (2010) A comparison method of silver nanoparticles prepared by the gamma irradiation and in situ reduction methods. Bull Korean Chem Soc 31(7): 1993–1996

Li Y, Wu Y, Ong BS (2005) Facile synthesis of silver nanoparticles useful for fabrication of high-conductivity elements for printed electronics. J Am Chem Soc 127(10): 3266–3267

Mallick K, Witcomb M, Scurrell M (2006) Silver nanoparticle catalysed redox reaction: an electron relay effect. Mater Chem Phys 97(2–3):283–287

Munro CH, Smith WE, Garner M, Clarkson J, White PC (1995) Characterization of the surface of a citrate-reduced colloid optimized for use as a substrate for surface-enhanced resonance Raman scattering. Langmuir 11(10):3712–3720

Patil SS, Dhumal RS, Varghese MV, Paradkar AR, Khanna PK (2009) Synthesis and antibacterial studies of chloramphenicol loaded nano-silver against *Salmonella typhi*. Synth React Inorg M 39(2):65–72

Qin Y, Ji X, Jing J, Liu H, Wu H, Yang W (2010) Size control over spherical silver nanoparticles by ascorbic acid reduction. Colloids Surf A 372(1–3):172–176

Rivas L, Sanchez-Cortes S, Garcia-Ramos JV, Morcillo G (2001) Growth of silver colloidal particles obtained by citrate reduction to increase the Raman enhancement factor. Langmuir 17(3):574–577

Ru ECL, Etchegoin PG (2009) Principles of surface-enhanced Raman spectroscopy and related plasmonic effects. Elsevier Science & Technology Books, New York

Schluecker S, Kiefer W (2010) Surface enhanced Raman spectroscopy: analytical biophysical and life science applications. Wiley, New York

Schmidt H, Bich Ha N, Pfannkuche J, Amann H, Kronfeldt H-D, Kowalewska G (2004) Detection of PAHs in seawater using surface-enhanced Raman scattering (SERS). Mar Pollut Bull 49(3):229–234

Sondi I, Goia DV, Matijević E (2003) Preparation of highly concentrated stable dispersions of uniform silver nanoparticles. J Colloid Interface Sci 260(1):75–81

Suh JS, DiLella DP, Moskovits M (1983) Surface-enhanced Raman spectroscopy of colloidal metal systems: a two-dimensional phase equilibrium in *p*-aminobenzoic acid adsorbed on silver. J Phys Chem 87(9):1540–1544

Thanh NTK, Green LAW (2010) Functionalisation of nanoparticles for biomedical applications. Nano Today 5(3):213–230

Wang H, Qiao X, Chen J, Ding S (2005) Preparation of silver nanoparticles by chemical reduction method. Colloids Surf A 256(2–3):111–115

Wiley BJ, Im SH, Li ZY, McLellan J, Siekkinen A, Xia Y (2006) Maneuvering the surface plasmon resonance of silver nanostructures through shape-controlled synthesis. J Phys Chem B 110(32):15666–15675

Xu H, Bjerneld EJ, Käll M, Börjesson L (1999) Spectroscopy of single hemoglobin molecules by surface enhanced Raman scattering. Phys Rev Lett 83(21):4357–4360

Yaffe NR, Blanch EW (2008) Effects and anomalies that can occur in SERS spectra of biological molecules when using a wide range of aggregating agents for hydroxylamine-

reduced and citrate-reduced silver colloids. Vib Spec 48(2):196–201

Yang G, Lin Q, Wang C, Li J, Wang J, Zhou J, Wang Y, Wang C (2012) Synthesis and characterization of dextran-capped silver nanoparticles with enhanced antibacterial activity. J Nanosci Nanotechnol 12(5):3766–3774

Yin B, Ma H, Wang S, Chen S (2003) Electrochemical synthesis of silver nanoparticles under protection of poly(*N*-vinylpyrrolidone). J Phys Chem B 107(34):8898–8904